Shell model plus cluster description of negative parity states in ^{212}Po

D. S. Delion,[1,2,3] R. J. Liotta,[4] P. Schuck,[5,6] A. Astier,[7] and M.-G. Porquet[7]

[1] *"Horia Hulubei" National Institute of Physics and Nuclear Engineering, 407 Atomiştilor, Bucharest-Măgurele, RO-077125, România*

[2] *Academy of Romanian Scientists, 54 Splaiul Independenţei, Bucharest, RO-050085, România*

[3] *Bioterra University, 81 Gârlei, Bucharest, RO-013724, România*

[4] *KTH, Alba Nova University Center, SE-10691 Stockholm, Sweden*

[5] *IPN, IN2P3/CNRS and Université Paris-Sud, F-91406 Orsay, France*

[6] *LPMMC, CNRS and Université Joseph Fourier, F-38042 Grenoble Cedex 9, France*

[7] *CSNSM, IN2P3/CNRS and Université Paris-Sud, F-91405 Orsay, France*

(Received 16 February 2012; revised manuscript received 15 May 2012; published 7 June 2012)

The intraband electromagnetic transitions in ^{210}Po and ^{210}Pb are well described within the shell model approach. In contrast, similar transitions in ^{212}Po are one order of magnitude smaller than the experimental values, suggesting the existence of an α-cluster component in the structure of this nucleus. To probe this assumption we introduced Gaussian-like components in the single-particle orbitals. We thus obtained an enhancement of intraband transitions, as well as a proper description of the absolute α-decay width in ^{212}Po. We analyzed the recently measured unnatural parity states I^- in ^{212}Po in terms of the collective octupole excitation in ^{208}Pb coupled to positive parity states in ^{210}Pb. They are connected by relatively large dipole transitions to yrast positive natural parity states. We described $E1$ transitions by using the same α-cluster component and an effective neutron dipole charge $e_\nu = -eZ/A$. $B(E2)$ values and absolute α-decay width in ^{212}Po are simultaneously described within the shell model plus a cluster component depending upon one free strength parameter.

DOI: 10.1103/PhysRevC.85.064306 PACS number(s): 21.60.Jz, 23.20.Js, 23.60.+e, 27.80.+w

I. INTRODUCTION

The nucleus ^{212}Po, with two neutrons and two protons outside the ^{208}Pb double magic core, has been a playing ground for methods and models which include the α particle as an elementary degree of freedom. In α-decay processes the α particle was considered as a cluster moving around the ^{208}Pb core, since the time when Gamow proposed the penetrability theory up to a time in the early 1960s, when it was realized that there were strong limitations with the Gamow theory if absolute decay widths were to be evaluated. In Ref. [1] it is concluded that a proper treatment of the absolute decay width would require a microscopic (shell model) framework where configuration mixing would play an important role. This conclusion was reached after calculations with only very few configurations, which was at the limit of the computing facilities at that time. These calculations showed that the corresponding absolute decay width could be wrong (too small) by as much as six orders of magnitude in comparison with the experimental data. It was in the late 1970s that this computing limitation could be overcome, showing that indeed the inclusion of many configurations increases the value of the absolute decay width by more than four orders of magnitude [2]. Shortly afterwards it was shown that the physical reason behind that big increase is that through such configurations one describes the clustering of the two neutrons and the two protons that eventually become the α particle [3]. Yet, the calculated width was still two orders of magnitude too small. The additional inclusion of proton-neutron configurations, and the corresponding clustering, improves this value but only by factor of about 5 [4]. Only a theory where combined shell- and cluster-model configurations were considered could reproduce the absolute decay width [5,6]. The amount of the cluster component in this theory was as large as 30%. This may justify extreme cluster models, where the states of ^{212}Po are explained as a result of an α particle moving around the ^{208}Pb core [7–10]. In fact the α-cluster model has shown to be able to reproduce well many levels in ^{212}Po, and it is been applied at present even to describe properties of spherical as well as deformed nuclei [11]. But it is important to point out that shell model approaches have been also used to calculate some properties of excited states of ^{212}Po [12,13]. While the energies of the yrast states are mostly found to be close to the experimental ones, these calculations cannot reproduce the large experimental $E2$ transition strengths [13], which are well accounted for from the α clustering [8–10].

A recent experiment evidenced several levels of unnatural parity, organized in two multiplets $4^-, 6^-, 8^-$ with almost degenerate energies of 1.8 and 2.0 MeV, respectively, plus an isolated state 10^- at 2.46 MeV. They are strongly connected by $E1$ transitions to the corresponding $4^+, 6^+, 8^+, 10^+$ states, respectively [14,15]. These states cannot be fully described as an α cluster moving around the ground state, since in such a model the parity of a level is $(-1)^{l_\alpha}$, where l_α is the angular momentum of the α particle. That is, only natural parity states are prone to be treated within straightforward α-particle models. To circumvent this problem it was proposed, very soon after Ref. [14] appeared, a coupled channel α-particle model, which allows the α particle to couple to the ^{208}Pb core in an excited 3^- state [16].

There is another fully microscopic possibility of explaining the strong $E1$ transitions mentioned above. As pointed out in Ref. [15], the collective particle-hole 3^- state in ^{208}Pb [14] may couple to two-particle states to induce the doublet of states connected by the $E1$ transitions, in a fashion similar to what

was found in the Gd region [17]. In this paper we will apply such a particle-vibration coupling scheme trying to describe the structure of ^{212}Po measured in Ref. [14].

The formalism is presented in Sec. II. Applications are in Sec. III and a summary and conclusions are in Sec. IV.

II. THE FORMALISM

The almost degenerate unnatural parity multiplet $I^- = 4^-, 6^-, 8^-$ in ^{210}Po was detected and interpreted as a pure two-proton configuration $(\pi h\frac{9}{2}^+ \otimes \pi j\frac{15}{2}^-)_{I^-}$ [14] [see Table I for the single-particle (sp) states in ^{208}Pb]. The degeneracy of the multiplet was explained in terms of a surface delta interaction which showed, as expected, that the matrix elements connecting such pairs are very small. This is in contrast to the matrix elements connecting natural parity pairs carrying, e.g., spin and parity I^-, where I is an odd spin. The same feature was predicted in ^{210}Pb, where a similar multiplet would appear as the result of the two-neutron configuration $(\nu g\frac{9}{2}^- \otimes \nu i\frac{13}{2}^+)_{I^-}$, but this was not observed yet.

Therefore, it would be appealing to interpret the two bands of unnatural parity states $I^- = 4^-, 6^-, 8^-$ in ^{212}Po as two multiplets of proton and neutron origin, respectively. This interpretation is endorsed by the zeroth-order energy of the states. With the sp energies of Table I one finds that they would lie at 3.13 and 3.37 MeV, respectively. Thus, their relative distance is correct and one can imagine an interaction pushing them to the experimental position. However, this simple description fails in providing the correct $B(E1)$ values corresponding to the decay from the multiplets to the natural positive parity states in ^{212}Po, which are built as neutron pairs carrying angular momentum and parity I^+ times proton pairs in the ground state [18]. In this framework the $B(E1)$ values from the proton multiplet to the corresponding I^+ states vanish. Moreover, the $E1$ transitions from the neutron multiplet also vanish since no neutron pair coupled to angular momentum 1^- can be built, as can be seen in Table I.

However, a similar excitation can be built as a three-particle one-hole (3p-1h) excitation. Many shell model calculations without including core excitations have been performed in ^{212}Po predicting a large number of levels (see Ref. [12] and references therein). Most of the available experimental data were thus well reproduced, although many calculated levels have not been observed yet. In particular, Ref. [12] predicts a 3^- state at 1.952 Mev, while in recent experimental data [15] a 3^- state was found at 1.537 MeV. This probably is a fraction of the collective ^{208}Pb(3_1^-) state at 2.6 MeV. There are strong indications of other core excited states in ^{212}Po. As pointed out in Ref. [15], there are a number of pairs of states with different parities which are strongly connected by $E1$ transitions. These states cannot be explained within the shell model without including core excitations. In fact, there are examples of such states in the Gd region, although the corresponding $E1$ transitions are not exceptionally strong (for details see Ref. [15]). The aim of this paper is to show that the main characteristic of these pairs of states is that the normal parity ones correspond to two-neutron excitations, i.e., states of angular momentum J and parity $(-1)^J$ of the form

$$|^{212}\mathrm{Po}(J^+)\rangle = |^{210}\mathrm{Pb}(J^+) \otimes {}^{210}\mathrm{Po(g.s.)}\rangle, \tag{2.1}$$

while the unnatural parity states are of the form

$$|^{212}\mathrm{Po}(I^-)\rangle = |[^{210}\mathrm{Pb}(J^+) \otimes {}^{210}\mathrm{Pb}(3^-)]_{I^-} \otimes {}^{210}\mathrm{Po(g.s.)}\rangle. \tag{2.2}$$

It is worthwhile to point out that the two additional protons in ^{210}Po(3^-), as compared to the ^{208}Pb core, induce a softening of the collective state with a lowering of the energy well below 2.6 MeV [15].

TABLE I. Single-particle proton (left) and neutron (right) levels in ^{208}Pb obtained by using the Blomqvist-Wahlborn set of Woods-Saxon parameters [22]. They are labeled from bottom to top in increasing energy order. Magic numbers are indicated.

n	l_π	j_π	ϵ_π (MeV)	n	l_ν	j_ν	ϵ_ν (MeV)
		$Z = 126$					
11	1	$p1/2^-$	0.47	12	4	$g7/2^+$	− 0.74
10	3	$f5/2^-$	− 0.53	11	0	$s1/2^+$	− 1.37
9	1	$p3/2^-$	− 0.70	10	7	$j15/2^-$	− 1.86
8	6	$i13/2^+$	− 1.86	9	2	$d5/2^+$	− 2.04
7	3	$f7/2^-$	− 3.55	8	6	$i11/2^+$	− 2.77
6	5	$h9/2^-$	− 3.80	7	4	$g9/2^+$	− 3.90
		$Z = 82$				$N = 126$	
				6	1	$p1/2^-$	− 7.39
5	0	$s1/2^+$	− 8.72	5	3	$f5/2^-$	− 8.06
4	2	$d3/2^+$	− 9.11	4	1	$p3/2^-$	− 8.33
3	5	$h11/2^-$	− 9.28	3	6	$i13/2^+$	− 8.55
2	2	$d5/2^+$	− 11.05	2	3	$f7/2^-$	− 10.47
1	4	$g7/2^+$	− 12.38	1	5	$h9/2^-$	− 10.67
		$Z = 50$				$N = 82$	

TABLE II. Energies of the pairing (yrast) states ^{210}Pb(J^+) (in MeV) referred to the ^{208}Pb(g.s.) core extracted from experiment [24,25].

J^+	0	2	4	6	8	10
$\omega(^{210}\mathrm{Pb}(J^+))$	−9.122	−8.322	−8.024	−7.929	−7.844	−7.316

A. Shell model natural parity states

As in Ref. [18], we will first evaluate the two-particle states by using the Tamm-Dankoff appproximation (TDA). The two-neutron state carrying angular momentum J needed to evaluate the natural parity states in Eq. (2.1) is given by

$$|\Psi_{J^+}(^{210}\mathrm{Pb})\rangle = \Gamma^\dagger_{JM}(\nu 1)|\Psi(^{208}\mathrm{Pb})\rangle, \tag{2.3}$$

where $\Gamma^\dagger_{JM}(\nu n)$ is the creation operator of the lowest correlated two-neutron state, with the eigenvalue index $n = 1$. In the two-neutron case of ^{210}Pb it is

$$\Gamma^\dagger_{JM}(\nu 1) = \sum_{j_1 \leqslant j_2} X^{(1)}_J(\nu j_1 j_2)\overline{A}^\dagger_{JM}(\nu j_1 j_2). \tag{2.4}$$

In this equation X is the TDA two-particle wave function amplitude and the bare two-particle creation operator is defined by

$$\begin{aligned}\overline{A}^\dagger_{JM}(\tau j_1 j_2) &= \frac{1}{\Delta_{j_1 j_2}}(a^\dagger_{\tau j_1} \otimes a^\dagger_{\tau j_2})_{JM} \\ \Delta_{j_1 j_2} &\equiv \sqrt{1+\delta_{j_1 j_2}},\end{aligned} \tag{2.5}$$

where $a^\dagger_{\tau j}$ is the sp creation operator corresponding to a particle moving in a Woods-Saxon mean field. The index τ labels protons ($\tau = \pi$) as well as neutrons ($\tau = \nu$). In the same fashion one evaluates the two-proton ground state of ^{210}Po.

The two-particle wave function amplitudes X will be evaluated by using the Hamiltonian

$$\hat{H}_\tau = \sum_j \epsilon_{\tau j}\hat{N}_{\tau j} + \hat{H}_{P\tau}, \tag{2.6}$$

where we introduced the pairing Hamiltonian

$$\hat{H}_{P\tau} = -\sum_{J^+} G_{J^+}(\tau)\hat{J}[P^\dagger_{J^+}(\tau) \otimes \tilde{P}_{J^+}(\tau)]_0, \tag{2.7}$$

in terms of the pair operator defined as

$$P^\dagger_{J^+M}(\tau) = \sum_{j_1 \leqslant j_2} \frac{2q_J(\tau j_1 j_2)}{\Delta_{j_1 j_2}}\overline{A}^\dagger_{J^+M}(\tau j_1 j_2). \tag{2.8}$$

Here, the factor $q_J(\tau j_1 j_2)$ is proportional to the reduced matrix element of the multipole operator, i.e.,

$$q_J(\tau j_1 j_2) = \frac{1}{\hat{J}}\langle \tau j_1 || Q_J || \tau j_2\rangle. \tag{2.9}$$

The interaction strength $G_{J^+}(\tau)$ will be obtained by fitting the two-particle binding energy of the yrast state with angular momentum J^+. In Ref. [18], this formalism was used in order to obtain the positive parity states. Indeed, from Table II of Ref. [18] it can be seen that basic states in ^{210}Po, ^{210}Pb, and ^{210}Bi are well reproduced. At the same time, one sees from Table III of the same reference that the low-lying states in ^{212}Po are reasonably described without any additional parametrization.

B. Shell model unnatural parity states

In this subsection we will briefly present the formalism to describe the coupling between the two-neutron states and the particle-hole 3^- mode. The wave function (2.2) can be viewed as having the form

$$|^{212}\mathrm{Po}(I^-)\rangle = |^{210}\mathrm{Pb}(I^-) \otimes {}^{210}\mathrm{Po(g.s.)}\rangle, \tag{2.10}$$

where

$$|^{210}\mathrm{Pb}(I^-)\rangle = |\Psi_{I^-}(^{210}\mathrm{Pb})\rangle = \Omega^\dagger_{I^-M}|\Psi(^{208}\mathrm{Pb})\rangle, \tag{2.11}$$

and

$$\Omega^\dagger_{I^-M} = \sum_{J=I,I\pm 2} Z_I(J)[\Gamma^\dagger_{3^-}(1) \otimes \Gamma^\dagger_{J^+}(\nu 1)]_{I^-M}. \tag{2.12}$$

Here, we introduced the collective p-h creation operator

$$\Gamma^\dagger_{3^-}(n) = \sum_{\tau j_1 j_2} \mathcal{X}^{(n)}_{3^-}(\tau j_1 j_2)B^\dagger_{3^-\mu}(\tau j_1 j_2), \tag{2.13}$$

where n is the eigenvalue index and the p-h pair operator is given by

$$B^\dagger_{3^-\mu}(\tau j_1 j_2) \equiv (a^\dagger_{\tau j_1} \otimes \tilde{a}_{\tau j_2})_{3^-\mu}. \tag{2.14}$$

We evaluated the metric matrix of the basis defining the $\Omega^\dagger$ operator. It turns out that it is rather close to unity and therefore the Pauli correlations are relatively small within the multistep shell model (MSM) approach [18,19].

For the evaluation of the p-h amplitudes $\mathcal{X}^{(n)}_{3^-}$ we will use the standard octupole-octupole interaction

$$\hat{H}_{Q\tau\tau'} = -F_{3^-}(\tau\tau')\hat{3}[Q^\dagger_{3^-}(\tau) \otimes \tilde{Q}_{3^-}(\tau')]_0, \tag{2.15}$$

in terms of the octupole operator

$$Q^\dagger_{3^-\mu}(\tau) = \sum_{j_1 j_2} q_3(\tau j_1 j_2)B^\dagger_{3^-\mu}(\tau j_1 j_2). \tag{2.16}$$

We neglected the random phase approximation (RPA) correlations [20]. Our calculations show that for the 3^- state in ^{208}Pb at $E = 2.615$ MeV such correlations are not very important. The sum of the backward amplitudes squared gives the value $\sum_{\tau j_1 j_2}[Y^{(1)}_{3^-}(\tau j_1 j_2)]^2 \approx 0.15$. Our results will show to what extent the TDA approximation (2.13) is able to describe the unnatural parity states in ^{212}Po.

TABLE III. The MSM interaction energies $E_{\mathrm{int}} = \Delta(^{210}\mathrm{Pb}(J^+), {}^{210}\mathrm{Po(g.s.)})$ extracted from experiment as described in the text. Energies are in MeV and referred to the ^{208}Pb(g.s.).

J^+	0	2	4	6	8
E_{int}	−1.438	−1.511	−1.434	−1.304	−1.340

The corresponding energies will be obtained by using effective interaction matrix elements extracted from experiment [17]. We notice that in Eq. (2.2) the energy of the unnatural parity states can be written as a sum of the energies corresponding to the pairing states ^{210}Pb(J^+) and ^{210}Po(g.s.) plus the energy of the particle-hole vibration state ^{210}Pb(3^-). In addition one has to add the energies Δ provided by the interaction among all these degrees of freedom. That is,

$$\begin{aligned} &E(^{212}\mathrm{Po}(I^-)) \\ &= \omega(^{210}\mathrm{Pb}(J^+)) + \omega(^{208}\mathrm{Pb}(3^-)) + \omega(^{210}\mathrm{Po}(\mathrm{g.s.})) \\ &\quad + \Delta(^{210}\mathrm{Po}(\mathrm{g.s.}),\ ^{208}\mathrm{Pb}(3^-); 3^-) + \Delta(^{210}\mathrm{Pb}(J^+), \\ &\quad \times\ ^{210}\mathrm{Po}(\mathrm{g.s.}); J^+) + \Delta(^{210}\mathrm{Pb}(J^+),\ ^{208}\mathrm{Pb}(3^-); I^-). \end{aligned} \tag{2.17}$$

All these energies will be taken from experimental data, as will be seen in the applications below, except the last term, for which there is not enough data to allow a reliable extraction of the value of Δ. Instead we will evaluate this number by using the multistep shell model [19], where the two-body interaction matrix elements are replaced by the corresponding energies and wave functions. In Ref. [19] the fourparticle case in terms of a two- times two-particle basis was analyzed. Proceeding in the same fashion one obtains for our particle-hole times two-particle case the expression

$$\begin{aligned} &\Delta(^{210}\mathrm{Pb}(J^+),\ ^{208}\mathrm{Pb}(3^-); I^-) \\ &= -\sum_{ijkl}[\omega(^{210}\mathrm{Pb}(J^+)) + \omega(^{208}\mathrm{Pb}(3^-)) - \epsilon_k - \epsilon_j \\ &\quad -\epsilon_l + \epsilon_i] \times \mathcal{X}_{3^-}(ij;\mathrm{Pb}(3^-))\mathcal{X}_{3^-}(ik;\mathrm{Pb}(3^-))\overline{X}_{J^+}(kl; \\ &\quad \times\ ^{210}\mathrm{Pb}(J^+))\overline{X}_{J^+}(jl;\ ^{210}\mathrm{Pb}(J^+))7(2J^+ + 1) \\ &\quad \times \begin{Bmatrix} i & j & 3^- \\ k & l & J^+ \\ 3^- & J^+ & I^- \end{Bmatrix}. \end{aligned} \tag{2.18}$$

where the index i labels a hole state and j, k, l label particle states. The quantities X are the TDA wave function amplitudes, overlined amplitudes are defined in the Appendix, and the rest of the notation is standard.

C. α-clustering component

It is known that the shell model (SM) estimate of the α-decay width, even including a very large number of configurations, underestimates the experimental value of ^{212}Po by several orders of magnitude [2]. Even the introduction of narrow Gamow resonances is able to describe only 1% of the decay width [18]. On the other hand, the shell model $B(E2)$ values in the same nucleus are similar to those in ^{210}Pb, but are one order of magnitude smaller with respect to the experimental data. In order to explain these discrepancies one can add to the sp SM radial wave function a cluster component for each angular momentum,

$$\psi_l(r) = \psi_l^{(\mathrm{SM})}(r) + \psi_l^{(\mathrm{clus})}(r), \tag{2.19}$$

where for simplicity of notation we dropped the isospin index. We use the standard expansion of the SM component in terms of spherical harmonic oscillator (ho) wave functions, with the standard ho parameter $\beta_0 = M_N\omega/\hbar$, and $\hbar\omega = 41A^{-1/3}$,

$$\psi_l^{(\mathrm{SM})}(r) = \sum_{N\leqslant N_0} b_{nl}(-)^n\mathcal{R}_{nl}^{(\beta_0)}(r). \tag{2.20}$$

The phase factor $(-)^n$ ensures a common sign of the spherical ho wave functions at large distances.

Notice that we can use as a cluster component similar sp wave functions, i.e. spherical ho functions, with a principal quantum number larger than the maximal value $N > N_0 = 5$ for protons and $N > N_0 = 6$ for neutrons (see Table I), i.e.,

$$\psi_l^{(\mathrm{clus})}(r) = \sum_{N} c_{nl}(-)^n\mathcal{R}_{nl}^{(\beta)}(r), \tag{2.21}$$

There are two ways to determine the expansion coefficients c_{nl}.

(a) First, one can simultaneously determine b_{nl} and c_{nl} in Eqs. (2.20) and (2.21) by diagonalizing the Woods-Saxon mean field and normalizing to unity the wave function (2.19). A mixed basis (2.19) with two different ho parameters was used in Ref. [6]. By using a smaller ho parameter for the cluster components (2.21), i.e., $\beta < \beta_0$, one obtains an enhancement of the wave function tail, and thus of the decay width. The energies of bound sp states and narrow resonances are not affected by this procedure. Only the level density of low-lying sp states in the continuum, which increases, is affected.

(b) It is also possible to diagonalize the residual two-body interaction between protons and neutrons. For this purpose, the authors of Ref. [5] used a basis containing Gaussian-like sp wave functions as cluster components, i.e.,

$$\psi_l^{(\mathrm{clus})}(r) = \mathcal{N}_l^{(\mathrm{clus})}e^{-\beta_c(r-r_0)^2/2}, \tag{2.22}$$

where the sp ho parameter β_c is connected to the α-particle ho parameter by the relation $4\beta_c = \beta_\alpha = 0.513$ fm^{-2}, which takes into account the fact that the α-particle wave function is a product of two proton and two neutron wave functions. In order to ensure proper normalization, the SM component should be multiplied by the factor $\mathcal{N}_l^{(\mathrm{SM})} = \sqrt{1 - [\mathcal{N}_l^{(\mathrm{clus})}]^2}$.

Let us also mention that the single-particle harmonic-oscillator parameter $\beta_0 \approx 0.16$ fm^{-2} is rather close to $\beta_c/4 = 0.13$ fm^{-2} and therefore the induced spuriosity is relatively small. We have chosen $r_0 = 1.2A^{1/3}$, i.e., the standard bulk value.

It is worthwhile to mention that the expansion of the Gaussian function in Eq. (2.22) in terms of spherical harmonic-oscillator functions [Eq. (2.21)] is very convergent. Thus, in Fig. 1(a), the Gaussian (2.22) is plotted by a solid line, while dot-dashed lines denote various terms entering the expansion (2.21) corresponding to the angular momentum $l = 5$. In Fig. 1(b) we give the coefficients c_{nl} for various angular momenta $l = 0, 1, \ldots, 8$. Notice that the maximal value of these distributions corresponds to a large value of the principal quantum number $N = 2n + l \in [8, 10]$. In this way the overlap between $\psi_l^{(\mathrm{SM})}$ are $\psi_l^{(\mathrm{clus})}$ is relatively small.

The product of two proton and two neutron single-particle wave functions can be written as a product between the relative and center of mass (cm) wave functions for both terms (2.20) and (2.21) [21]. The overlap with the α-particle wave function gives the so-called preformation amplitude in terms of the cm

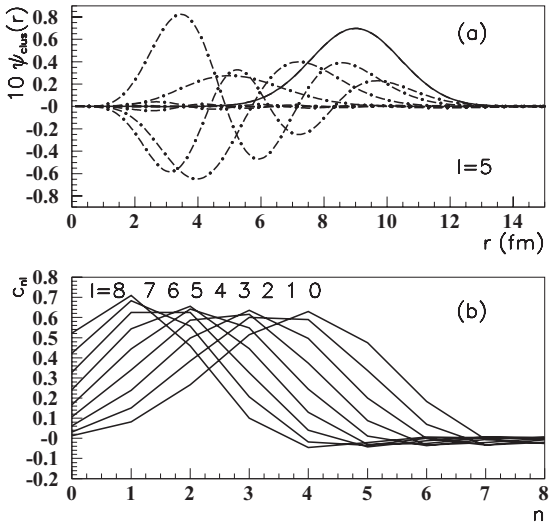

FIG. 1. (a) A Gaussian centered on the nuclear surface (solid line), given by Eq. (2.22), and its spherical harmonic oscillator components (dot-dashed lines). (b) The expansion coefficiens (2.21) of the Gaussian (2.22) for different angular momenta l.

radius

$$\Psi(R) = \Psi_{\rm cm}^{\rm (SM)}(R) + \Psi_{\rm cm}^{\rm (clus)}(R), \tag{2.23}$$

where for simplicity we neglected the interference terms. The theoretical decay width from a spherical nucleus has the following standard representation [21]:

$$\Gamma_{th} = \hbar v \left[\frac{\Psi(R)}{G_0(R)}\right]^2, \tag{2.24}$$

in terms of the irregular monopole Coulomb function $G_0(R)$ and the relative velocity of emitted fragments v. We will estimate the logarithm of the ratio between the theoretical and experimental decay widths, i.e.,

$$\log_{10}\frac{\Gamma_{th}}{\Gamma_{\rm exp}} = \log_{10}\Psi^2(R) - \log_{10}\left[\frac{G_0^2(R)}{\hbar v}\frac{1}{\Gamma_{\rm exp}}\right]. \tag{2.25}$$

Notice that the radial matrix element of the electric transition operator in a spherical ho basis behaves as

$$\left\langle \mathcal{R}_{nl}^{(\beta)} \middle| r^\lambda \middle| \mathcal{R}_{n'l'}^{(\beta)} \right\rangle \sim \left(\frac{N}{\beta}\right)^{\lambda/2}, \quad N = 2n + l. \tag{2.26}$$

As shown in Fig. 1(b), the decomposition of the cluster wave function given by Eq. (2.21) shows a significant spreading of the principal quantum number above the SM value, i.e., $N > N_0$. It thus becomes clear that the cluster component leads to an enhancement of the $B(E\lambda)$ value, since the reduced matrix element of the quadrupole operator is proportional to $N^{\lambda/2}$ [see Eq. (2.26)].

Therefore the cluster component ensures a simultaneous enhancement of both α-decay width and $B(E\lambda)$ value of the electromagnetic transitions in ^{212}Po.

III. NUMERICAL APPLICATION

We will use as a representation the sp states shown in Table I, which include the major shells $N = 4, 5$ for protons and $N = 5, 6$ for neutrons. Let us mention that the Blomqvist-Wahlborn set of Woods-Saxon parameters in this table gives the best description of single-particle levels in the four odd-A nuclei close to ^{208}Pb [22]; see also Fig. 2.15 of Ref. [23]. With this representation we evaluated the energies and wave functions of the correlated two-proton states in ^{210}Po and two-neutron states in ^{210}Pb. The positive parity states in ^{212}Po were estimated within the MSM procedure as in Ref. [18] without any additional parametrization. They are given in Fig. 2 by open symbols, while the corresponding experimental data are plotted by filled symbols. We found that the proton-neutron interaction is small and therefore the energies of positive parity states in ^{212}Po are close to the corresponding energy in ^{210}Pb. As seen in Fig. 2, the largest difference between these two sets of states is about 200 keV.

The challenge of the calculation is to evaluate the unnatural parity states 4^-, 6^-, and 8^- of ^{212}Po. The experimental data [14,15] display two groups of states, almost degenerated in energy, as two nearly parallel bands with almost constant values around $E = 1.8$ and 2.0 MeV (see the filled circles of Fig. 3). This means that in Eq. (2.12) one state with a given even spin J^+ is dominant, i.e., $Z_I(J) \sim \delta_{J;I,I\pm1}$, and each J value is able to create a triplet of almost degenerate states.

To perform the calculation of these states as precisely as possible we took the effective matrix elements from experiment, as mentioned above, by using Eqs. (2.17) and (2.18). The energies of the particle-hole and pairing modes, referred to the ^{208}Pb(g.s.) core, are [24,25] $\omega(^{208}\text{Pb}(3^-)) = 2.615$ MeV and $\omega(^{210}\text{Po(g.s.)}) = -8.782$ MeV. The values of $\omega(^{210}\text{Pb}(J^+))$ are given in Table II. The corresponding wave functions were evaluated as described above.

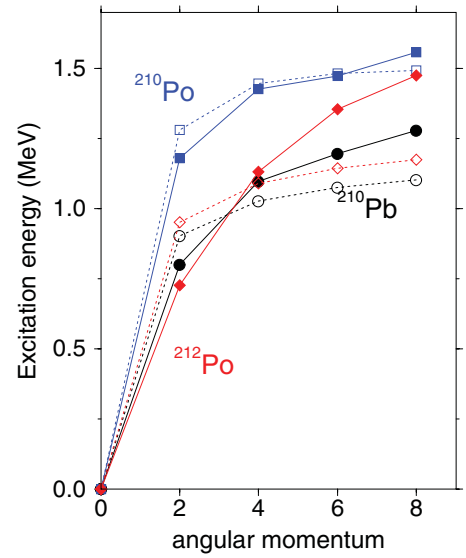

FIG. 2. (Color online) Energies of the positive parity states in ^{210}Pb (circles), ^{210}Po (squares), and ^{212}Po (diamonds), as a function of angular momentum. Experimental values are drawn with filled symbols and theoretical results [18] are drawn with open symbols.

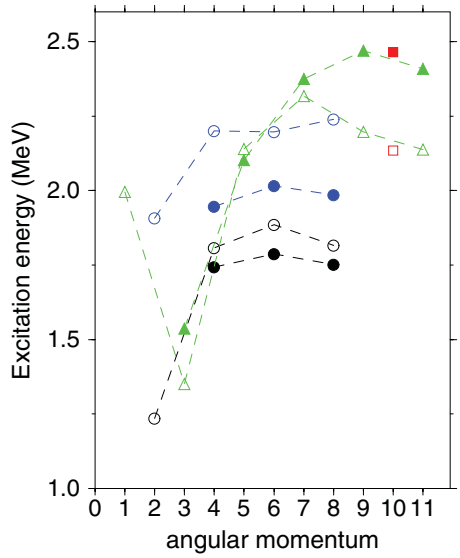

FIG. 3. (Color online) Energies of the negative parity states in ^{212}Po as a function of angular momentum. Experimental values [14,15] are drawn with filled symbols and theoretical predictions (this work) are drawn with open symbols.

The next quantities needed in Eq. (2.17) are the interaction energies Δ. We will evaluate them separately.

A. The interaction energy $\Delta(^{210}\text{Po(g.s.)}, ^{208}\text{Pb}(3^-); 3^-)$

The interaction between the pairing mode ^{210}Po(g.s.) and the particle-hole vibration ^{208}Pb(3^-), that is, the quantity $\Delta(^{210}\text{Po(g.s.)}, ^{208}\text{Pb}(3^-); 3^-)$, can be extracted from experimental data. To do this we assume that these collective modes are built upon each other such that $|^{210}\text{Po}(3^-)\rangle \approx |^{210}\text{Po(g.s.)} \otimes ^{208}\text{Pb}(3^-); 3^-\rangle$. Therefore the energy carried by the state ^{210}Po(3^-) is $E(^{210}\text{Po}(3^-)) = \omega(^{210}\text{Po(g.s.)}) + \omega(^{208}\text{Pb}(3^-)) + \Delta(^{210}\text{(g.s.)}, ^{208}\text{Pb}(3^-); 3^-)$. From experimental data [24] one has $E(^{210}\text{Po}(3^-)) = 2.387$ MeV. One has also to consider in this case of proton excitations the attractive Coulomb interaction between the two proton particles in the ^{210}Po(g.s.) mode and the proton hole in the ^{208}Pb(3^-) mode. This contribution is twice the value corresponding to the particle-hole contribution, which in this case we estimated to be -0.258 MeV (see Eq. (4.3) of Ref. [26]). Referring all energies to the core one finally obtains $\Delta(^{210}\text{Po(g.s.)}, ^{208}\text{Pb}(3^-); 3^-) = -0.745$.

TABLE V. Same as in Table IV, but for the energies of natural parity 3p-1h states I^-.

I^-	J^+	E_{MSM} (MeV)	$E(^{212}\text{Po}(I^-))$ (MeV)	$E_{\text{exp}}(^{212}\text{Po}(I^-))$ (MeV)
1^-	4^+	-0.116	1.995	
3^-	2^+	-0.356	1.350	1.537
5^-	6^+	-0.168	2.140	2.103
7^-	8^+	-0.137	2.318	2.374
9^-	8^+	-0.258	2.197	2.470
11^-	8^+	-0.317	2.137	2.409

B. The interaction energy $\Delta(^{210}\text{Pb}(J^+), ^{210}\text{Po(g.s.)}; J^+)$

In the evaluation of this quantity we assume $|^{212}\text{Po}(J^+)\rangle \approx |^{210}\text{Pb}(J^+) \otimes ^{210}\text{Po(g.s.)}\rangle$. Proceeding as above one obtains for the energy of this state the value $E(^{212}\text{Po}(J^+)) = \omega(^{210}\text{Pb}(J^+)) + \omega(^{210}\text{Po(g.s.)}) + \Delta(^{210}\text{Pb}(J^+), ^{210}\text{Po(g.s.)})$. We took the values of $E(^{212}\text{Po}(J^+))$ and the energies ω from experiment [24]. The resulting values of Δ are given in Table III.

C. The interaction energy $\Delta(^{210}\text{Pb}(J^+), ^{208}\text{Pb}(3^-); I^-)$

We evaluated this energy by using Eq. (2.18) with the single-particle energies given in Table I. This is the last contribution to the total energy $E(^{212}\text{Po}(I^-))$ given by Eq. (2.17). We summed up all these contributions and referred their values to the ground state of ^{212}Po. The values of $\Delta(^{210}\text{Pb}(J^+), ^{208}\text{Pb}(3^-); I^-)$ as well as $E(^{212}\text{Po}(I^-))$ are presented in Table IV. By using the same procedure we obtain the results for similar natural parity 3p-1h states having $I^\pi = 1^-, 3^-, 5^-, 7^-, 9^-$; they are given in Table V.

It is seen in Table IV that the experimental energies of the even-spin states (see the filled circles in Fig. 3) are fitted

TABLE IV. Calculated energies $E(^{212}\text{Po}(I^-))$ corresponding to the states $|^{212}\text{Po}(J^+)\rangle$ [Eq. (2.1)]. The MSM partial contribution is $E_{MSM} = \Delta(^{210}\text{Pb}(J^+), ^{208}\text{Pb}(3^-); I^-)$. Energies are in MeV and referred to ^{212}Po(g.s.). In the fifth column are the experimental energies, the SM $B(E1; I^- \to I^+)$ values with $e_\nu = -eZ/A$ are in the sixth column, and in the seventh column are the SM + cluster values. In the last column are the experimental $B(E1; I^- \to I^+)$.

I^-	J^+	E_{MSM} (MeV)	$E(^{212}\text{Po}(I^-))$ (MeV)	$E_{\text{exp}}(^{212}\text{Po}(I^-))$ (MeV)	$B(E1)^{(1)}_{th}$ (10^4 W.u.)	$B(E1)^{(2)}_{th}$ (10^4 W.u.)	$B(E1)_{\text{exp}}$ (10^4 W.u.)
2^-	2^+	-0.407	1.236		5	1	
	4^+	-0.204	1.907		15	63	
4^-	4^+	-0.303	1.808	1.744	9	11	25
	6^+	-0.107	2.201	1.946	2	4	11
6^-	6^+	-0.213	1.886	1.787	37	122	66
	8^+	-0.490	2.197	2.016	3	8	19
8^-	6^+	-0.489	1.816	1.751	43	148	200
	8^+	-0.215	2.240	1.986	8	24	
10^-	8^+	-0.360	2.135	2.465	2	1	18

within 150 keV, although the experimental tendency, where the states 6^- reach a maximun, is not reproduced. However, these differences are so small that they can be included within the general agreement of 150 keV beween theory and experiment.

One can see a nice agreement with the experimental values. It turns out that more than 90% of the contribution to Eq. (2.4) comes from the diagonal reduced matrix element with $j = j' = h9/2^-$ for protons and $j = j' = g9/2^+$ for neutrons (see Table I). The same combinations give the dominant contribution of the proton/neutron TDA amplitudes, i.e.,

$$\left| X^{(1)}_{J^+}\left(\tau\frac{9^\mp}{2}, \quad \tau\frac{9^\mp}{2}\right)\right| > 0.9, \quad \tau = \pi, \nu, \tag{3.1}$$

with $J^+ = 2^+, 4^+, 6^+, 8^+$.

We estimated the $B(E2)$ values according to Eq. (A3) by using the effective charges given by

$$e_\pi = e(1+\chi), \quad e_\nu = e\chi, \quad \chi = 1. \tag{3.2}$$

Let us mention that the polarization parameter $\chi = 1$ is suggested by systematic calculations, in particular by Ref. [13]. The corresponding numbers are shown in Table VI. In Ref. [8] the large $B(E2)$ values in ^{212}Po are reproduced within a pure cluster model. Here, one considers that the α cluster has a volume distribution. Anyway, an α particle can exist only on the nuclear surface and not inside. All microscopic estimates of the formation amplitude [2–6] indicate this feature. Thus, it is difficult to compare a pure volume cluster model with our shell model plus surface α cluster.

It has to be pointed out that the $B(E2)$ experimental values in ^{212}Po (the sixth column of Table VI) are one order of magnitude larger that the corresponding values in ^{210}Pb [15]. As we already mentioned, the previously computed $B(E2)$ values in ^{212}Po are one order of magnitude smaller.

This difference should be explained by an additional α-clustering component in Eq. (2.19). In order to determine the parameters of this component we first estimated the theoretical α-decay width by using the preformation amplitude (2.23) in Eq. (2.25). It turns out that the SM component underestimates the experimental value by three orders of magnitude. Since the SM preformation amplitude $\Psi_{\rm cm}(R)$ has a maximum around $r_0 = 1.2A^{1/3}$ [21], we adopted it as the the radius of the α-cluster distribution at the nuclear surface. As mentioned above, the ho parameter was taken to be four times the α-particle value $4\beta_c = \beta_\alpha = 0.513$ fm^{-2}. The only free parameter is the amplitude of the cluster factor, which we considered to be the same for all sp states. This approximation is justified, since practically only the states $\pi h9/2^-$ and $\nu g9/2^+$ provide

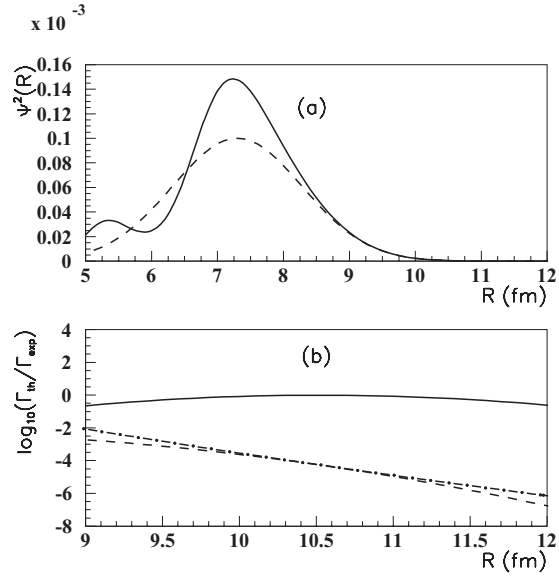

FIG. 4. (a) The α-particle preformation amplitude squared (2.23) (solid line) and its cluster part (dashed line).(b) The logarithm of the ratio between theoretical and experimental α-decay widths versus cm radius (solid line). The dashed and dot-dashed line are the two terms of Eq. (2.25), respectively.

a significant contribution. We fixed this parameter to reproduce the experimental value of the α-decay width, which provides the value $\mathcal{N}^{(\rm clus)} = 0.3$.

In Fig. 4(a) the preformation amplitude squared is shown (solid line) as well as the contribution of the cluster component (dashed line). In Fig. 4(b) the logarithm of the ratio between the theoretical and experimental decay widths is plotted as a function of the cm radius (solid line). One outstanding feature of this figure is the good agreement between the theoretical and experimental decay widths around the region of the geometrical touching configuration. Here the dependence upon the cm radius R is weak and therefore the decay width (2.24) practically does depend upon it in this region. This proves the validity of our calculation. The dashed and dot-dashed lines in Fig. 4 give the two terms of Eq. (2.25). The first (second) term corresponds to the internal (external) cm wave functions of the α particle. Thus, our approach is self-consistent because the derivatives of the two terms are almost equal and the final result practically does not depend upon the matching cm radius.

Notice that the value of the cluster normalization factor, $\mathcal{N}^{(\rm clus)} = 0.3$, is close to that given by Ref. [5]. Finally, we used this value in Eqs. (A1) and (2.19) to estimate the $B(E2)$

TABLE VI. Experimental and theoretical $B(E2)$ values in ^{210}Po (second and third columns), ^{210}Pb (fourth and fifth columns), and ^{212}Po (sixth and last columns) in Weiskopf units.

$J' \to J$	^{210}Po $B(E2)_{\rm exp}$	$B(E2)_{th}$	^{210}Pb $B(E2)_{\rm exp}$	$B(E2)_{th}$	^{212}Po $B(E2)_{\rm exp}$	$B(E2)_{th}$
$2 \to 0$	0.56(12)	6.7	1.4(4)	3.9		9.2
$4 \to 2$	4.6(2)	12.9	3.2(7)	3.5		20.8
$6 \to 4$	3.0(1)	8.9	2.2(3)	2.4	13.5(36)	14.4
$8 \to 6$	1.18(3)	3.9	0.62(5)	1.0	4.60(9)	5.8

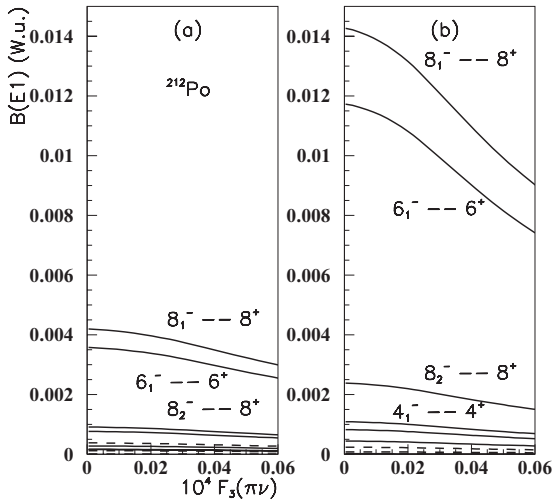

FIG. 5. (a) $B(E1)$ values for transitions $I^- \to I^+$ in Table IV versus the proton-neutron coupling strength $F_{3^-}(\pi\nu)$ for a vanishing α-clustering amplitude $\mathcal{N}^{(\mathrm{clus})} = 0$ (solid lines). The transitions between natural parity states $(I+1)^- \to I^+$ are given by dashed lines. (b) Same as in (a) but for $\mathcal{N}^{(\mathrm{clus})} = 0.3$.

values in ^{212}Po. The results are given in the last column of Table VI. One sees a nice agreement with respect to the experimental data.

We then proceeded to the evaluation of the $B(E1)$ values corresponding to the unnatural parity states. The theoretical neutron dipole charge is $e_\nu = -eZ/A$. In order to simplify the calculations we used equal proton and neutron octupole strengths, i.e., $F_{3^-}(\pi\pi) = F_{3^-}(\nu\nu)$. The proton-neutron octupole strength $F_{3^-}(\pi\nu)$ is determined by using Eq. (A10). Thus, the interval of values is given by

$$F_{3^-}(\pi\nu) \in \left[0, \left(S_\pi^{(1)} S_\nu^{(1)}\right)^{-1/2}\right], \tag{3.3}$$

where the quantities $S_\tau^{(1)}$ are the ones defined by Eq. (A9) for the lowest root $n = 1$. We analyzed the dependence of $B(E1)$ values versus the proton-neutron octupole strength. In Fig. 5(a) we give by solid lines $B(E1)$ values as functions of $F_{3^-}(\pi\nu)$, according to Eq. (A8), for transitions in Table IV. Here, we considered a vanishing α-cluster correction, i.e., $\mathcal{N}^{(\mathrm{clus})} = 0$ in Eq. (2.22). The largest transitions are explicitely labeled on the plot. One clearly sees that these dependencies are rather smooth, the strongest variation being lower than a factor of 2.

It is important to stress that one has opposite situations for $E1$ transitions between natural parity states $[(I+1)^- \to I^+$, i.e., $5^- \to 4^+, 7^- \to 6^+, 9^- \to 8^+]$ and unnatural parity states $[I^- \to I^+]$ even though the two sets of negative parity states are described by the same ansatz (2.12). In the first case, the two terms entering Eq. (A6) have the same sign, thus their difference leads to significantly smaller values. This feature can be seen in Fig. 5, where the dependence of the $B(E1)$ values upon the proton-neutron strength $F_{3^-}(\pi\nu)$ for these transitions is given by dashed lines.

The largest values of $B(E1)$, corresponding to $F_{3^-}(\pi\nu) = 0$, are given in the sixth column of Table IV. They are significantly smaller than the experimental values given in the last column.

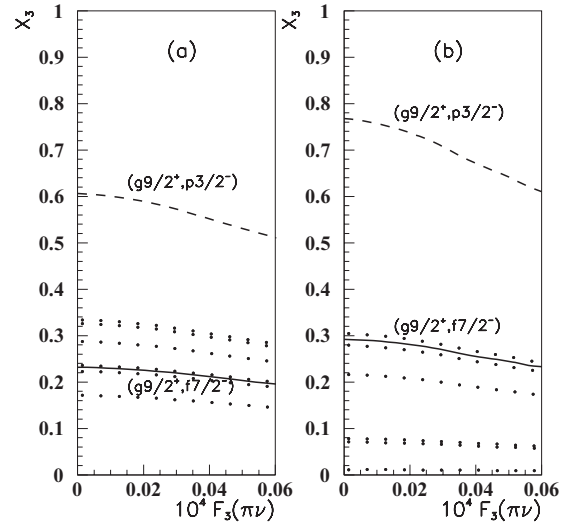

FIG. 6. (a) The largest octupole TDA amplitude, given by the neutron pair $(\nu g\frac{9}{2}^+ \otimes \nu p\frac{3}{2}^-)_{3^-}$, versus the proton-neutron coupling strength $F_{3^-}(\pi\nu)$ is drawn by a dashed line. Other important amplitudes are given by dotted lines. The TDA amplitude giving the leading contribution in $E1$ transitions, corresponding to the neutron p-h pair $(\nu g\frac{9}{2}^+ \otimes \nu f\frac{7}{2}^-)_{3^-}$, is plotted by a solid line. The α-clustering amplitude is $\mathcal{N}^{(\mathrm{clus})} = 0$. (b) Same as in (a), but for $\mathcal{N}^{(\mathrm{clus})} = 0.3$.

In Fig. 5(b) we plotted the same dependencies, but considering the same α-cluster correction reproducing the absolute value of the α-decay width, i.e., $\mathcal{N}^{(\mathrm{clus})} = 0.3$. One notices an important enhancement of these values. Indeed, the enhancement provided by the same cluster term given by Eq. (2.22) is given by the radial part of the reduced matrix elements, which according to Eq. (2.26), are proportional to $\sqrt{N}$.

The largest $B(E1)$ values, corresponding to $F_{3^-}(\pi\nu) = 0$, are shown in the sixth column of Table IV and they are, except for the last line, in reasonable agreement with the experimental data, given in the last column. Notice that the clustering enhancement increases with the value of the spin I. Indeed, Eq. (A6) shows that the dipole transition operator is proportional to I.

The 3^- state has a very collective character due to the fact that many components have significant amplitudes, larger than 0.3. It turns out that the dominant component is given by the particle-hole neutron amplitude $|\mathcal{X}_{3^-}^{(1)}(\nu g\frac{9}{2}^+, \nu p\frac{3}{2}^-)| > 0.5$ (see Table I). It is plotted in Fig. 6(a) by a dashed line versus the proton-neutron octupole strength for a vanishing α-clustering amplitude $\mathcal{N}^{(\mathrm{clus})} = 0$. One obtains an important enhancement for $\mathcal{N}^{(\mathrm{clus})} = 0.3$, as can be seen in Fig. 6(b).

Several other important amplitudes corresponding to various neutron pairs $(\nu j_1 \otimes \nu j_2)_{3^-}$ are plotted by dotted lines in Fig. 6(a). It turns out that only one specific two-neutron state plays an important role in the $E1$ transitions. Thus, in the dipole transition operator (A6) the dominant component is given by the particle-hole neutron pair $(\nu g\frac{9}{2}^+ \otimes \nu f\frac{7}{2}^-)_{3^-}$, with $\Delta j = 1$, in spite of the fact that the TDA amplitude corresponding to this pair is not the largest one, its value being less than 0.3. This amplitude is plotted in Fig. 6(a) by a solid line for a vanishing α-clustering amplitude $\mathcal{N}^{(\mathrm{clus})} = 0$. It has the same order of magnitude as in Ref. [20], although there the RPA

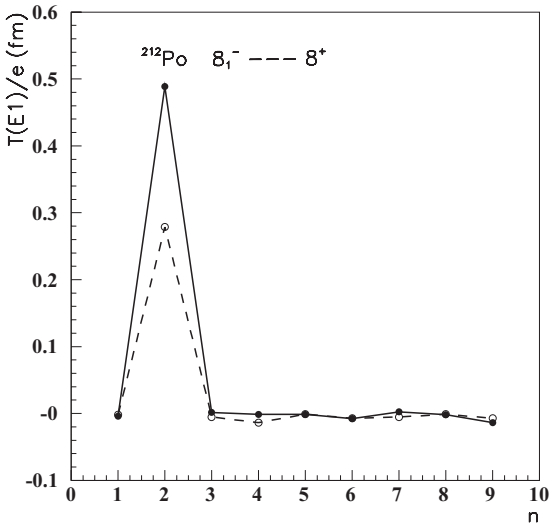

FIG. 7. The distribution of different terms in the $E1$ transition operator (A6) divided by the electric charge (in fm) versus the neutron state number for the strongest transition $8_1^- \to 8^+$ in ^{212}Po, by considering $\mathcal{N}^{(\mathrm{clus})} = 0$ (open circles connected by a dashed line). The maximum corresponds to the neutron dipole pair $(\nu g\frac{9}{2}^+ \otimes \nu f\frac{7}{2}^-)_{1^-}$. The dark circles connected with a solid line show the same dependence, but for $\mathcal{N}^{(\mathrm{clus})} = 0.3$.

was used. Its enhancement for $\mathcal{N}^{(\mathrm{clus})} = 0.3$ is not spectacular, as can be seen in Fig. 6(b), but the $B(E1)$ value strongly increases. Notice that for this combination the two terms of the dipole transition operator (A6) have opposite phases and their difference has a relatively large value. Finally let us mention that the amplitudes plotted by dotted lines are unchanged and even decrease when increasing the cluster amplitude, as can be seen from Fig. 6(b).

In order to visualize the contribution of different terms in the $E1$ transition operator (A6), we plotted them versus the neutron state number n for the strongest transition $8^- \to 8^+$. Thus, in Fig. 7 we give this distribution for those terms with an absolute value larger than 10^{-4} and a vanishing clustering $\mathcal{N}^{(\mathrm{clus})} = 0$, represented by open circles connected with a dashed line. The second state with the largest contribution corresponds to the neutron dipole pair $(\nu g\frac{9}{2}^+ \otimes \nu f\frac{7}{2}^-)_{1^-}$. One can see the enhancement of this peak by including the α-clustering term with $\mathcal{N}^{(\mathrm{clus})} = 0.3$ (dark circles connected by a solid line).

There is one exception, corresponding to the transition from the state $I = 10_1^-$, where the leading contribution is given by the term $(\nu i\frac{11}{2}^+ \otimes \nu f\frac{7}{2}^-)_{3^-}$ with $\Delta j = 2$. This feature explains why the transition from the state 10_1^- has a small value, in agreement with the experiment. It is worth mentioning that the two-neutron state 10^+ has a different structure compared to Eq. (3.1), since in ^{210}Pb it is

$$\left| X^{(1)}_{10^+}\left(\nu g\frac{9}{2}^+,\quad \nu i\frac{11}{2}^+\right)\right| > 0.9, \tag{3.4}$$

pushing its energy to a larger value (see Fig. 2), together with the energy of the corresponding state 10^- in ^{210}Pb.

TABLE VII. The ratios between the half-life of the α decay from the ground state and from excited natural parity states of ^{212}Po. In the second column are given experimental values [14] and in the third column are the theoretical estimates. In the last column are given similar theoretical values from Table VII (last column) of Ref. [27].

J	T_0/T_J (exp)	T_0/T_J	T_0/T_J [27]
2		26.1	24.2
4		48.9	44.7
6	12.0	17.5	15.4
8	0.6	1.8	1.7

Finally, let us mention that the ratios between the α-decay half-life from the ground state and from excited natural parity states of ^{212}Po, computed in Table VII by using the above described formalism, are in agreement with those predicted in Ref. [27].

IV. SUMMARY AND CONCLUSIONS

In this paper we have shown that the pairs of natural and unnatural parity states seen in ^{212}Po ([14,15]) appear as a result of two different mechanisms. The natural positive parity states are two-neutron excitations built upon the nucleus ^{210}Po(g.s.). We described these states by using a pairing Hamiltonian. The interaction strengths were fixed as usual, i.e., by fitting the energy of each multipolarity to the corresponding yrast state. It was found that the $B(E2)$ values in ^{210}Po are in good agreement with experimental data by using an effective neutron charge $e_\nu = e$. However, the shell-model predictions of the corresponding $B(E2)$ values in ^{212}Po are smaller than the experimental data by one order of magnitude. In order to explain this discrepancy we used a surface α-cluster component. It turns out that a cluster admixture of 30% is able to simultaneously describe $B(E2)$ and absolute α-decay width as already shown previously in Ref. [5]. $B(E2)$ values and absolute α-decay width in ^{212}Po are simultaneously described within the shell model plus a cluster component depending upon one free strength parameter.

We described the unnatural negative parity states in ^{212}Po as two-neutron excitations in ^{210}Pb coupled to the collective ph 3^- state in ^{208}Pb times ^{210}Po(g.s.). The energies of the corresponding I^- states are in reasonable agreement with the experimental data. The $B(E1)$ values are also in a reasonably good agreement with existing experimental data, by using an effective neutron charge $e_\nu = -eZ/A$ which is the theoretical neutron dipole charge.

Looking at the experimental spectrum of ^{212}Po (see Refs. [14,15]), one gets the impression that the story of two more or less parallel bands of unnatural parity states repeats itself for the odd-spin states $(5^+, 7^+, 9^+)$ only $\sim$2 MeV higher. These states are connected by strong $E1$ transitions to the corresponding negative natural parity states $J^- = 5^-, 7^-, 9^-$, analagous to what happens in the case of the even spins described in this work. In order to describe these transitions one has to suppose for odd-spin states a similar structure to Eq. (2.12), i.e., $I^+ = (3^- \otimes J^-)_{I^+}$. The only difference is that the natural parity states J^- are again given by Eq. (2.12). In

other words, the odd-spin unnatural parity states may be based on the double excitation of the 3^- state in ^{208}Pb; see, e.g., Ref. [28]. The analysis of odd-spin unnatural parity states is under way.

ACKNOWLEDGMENTS

This work was supported by Project No. PN-II-ID-PCE-2011-3-0092 of the Romanian Ministry of Education and Research, IN2P3–IFIN-HH Agreement, and by the Wenner-Gren Foundation.

APPENDIX

We give in this Appendix some analytic relations used in our calculations.

(A) The intraband $E\lambda\colon J' \to J$ transition is described by the reduced matrix element

$$\langle J||\hat{T}_\lambda||J'\rangle = \sum_{\tau=\pi,\nu} e_\tau (-)^{\lambda+J}\hat{J}\hat{J}' \sum_{j_1 j_2 j_1' j_2'} \langle \tau j_1||\hat{T}_\lambda||\tau j_1'\rangle (-)^{j_1'-j_2} \times W(Jj_1J'j_1';j_2\lambda)\overline{X}^{(1)}_J(j_1j_2)\overline{X}^{(1)}_{J'}(j_1'j_2')\delta_{j_2j_2'}, \tag{A1}$$

where e_τ are the effective charges. We introduced the extended amplitude by

$$\begin{aligned}\overline{X}^{(n)}_J(\tau j_1 j_2) &= X^{(n)}_J(\tau j_1 j_2)\Delta_{j_1 j_2}, \quad j_1 \leqslant j_2 \\ &= X^{(n)}_J(\tau j_2 j_1)\Delta_{j_2 j_1}(-)^{j_1+j_2-J+1}, \quad j_1 > j_2.\end{aligned} \tag{A2}$$

The $B(E2)$ value is computed according to the following relation:

$$B(E2\colon J' \to J) = \frac{1}{2J'+1}\left|\langle J||\hat{T}_2||J'\rangle\right|^2. \tag{A3}$$

(B) The E1 transition operator is given by

$$\begin{aligned}\hat{T}_{1\mu} &= \sum_\tau e_\tau \sum_{k_1k_2}\frac{1}{\sqrt{3}}\langle \tau k_1||\mathbf{r}||\tau k_2\rangle (a^\dagger_{\tau k_1}\tilde{a}_{\tau k_2})_{1\mu} \\ &= \sum_\tau e_\tau \sum_{k_1k_2}\frac{1}{\sqrt{3}}\langle \tau k_1|r|\tau k_2\rangle\langle k_1||Y_1||k_2\rangle (a^\dagger_{\tau k_1}\tilde{a}_{\tau k_2})_{1\mu},\end{aligned} \tag{A4}$$

where we introduced the effective dipole charges

$$e_\pi = \frac{N}{A}, \quad e_\nu = -\frac{Z}{A}. \tag{A5}$$

Thus, one obtains

$$\begin{aligned}|\langle \Omega_{I^-}||\hat{T}_1||\Gamma^\dagger_{I^+}(1)\rangle| = |\langle \Gamma_{I^+}(1)||\hat{T}_1||\Omega^\dagger_{I^-}\rangle| \equiv T_1(\lambda^-, J^+; I^- \to I^+) = \sum_\tau e_\tau\sqrt{(2\lambda^-+1)(2J^++1)}(2I^++1) \\ \times \sum_{j_1\leqslant j_2}\sum_{j_3j_4}\frac{1}{\Delta_{j_1j_2}}X^{(1)}_{J^+}(\tau j_1j_2)\mathcal{X}^{(1)}_{\lambda^-}(\tau j_3j_4)\left|\overline{X}^{(1)}_{I^+}(\tau j_2j_3)\langle \tau j_1||\mathbf{r}||\tau j_4\rangle \begin{Bmatrix} j_1 & j_2 & J^+ \\ j_4 & j_3 & \lambda^- \\ 1^- & I^+ & I^-\end{Bmatrix}(-)^{j_3+j_4}\right. \\ \left. - \overline{X}^{(1)}_{I^+}(\tau j_1j_3)\langle \tau j_2||\mathbf{r}||\tau j_4\rangle \begin{Bmatrix} j_1 & j_2 & J^+ \\ j_3 & j_4 & \lambda^- \\ I^+ & 1^- & I^-\end{Bmatrix}\right|,\end{aligned} \tag{A6}$$

with $\lambda = 3$ and we explicitely indicated the parities. Notice that this relation is valid for any value of λ and different values of initial I^- and final spin I^+,

$$B(E1\colon I^- \to I^+) = \frac{1}{2I^-+1}[T_1(\lambda^-, J^+; I^- \to I^+)]^2. \tag{A7}$$

(C) The dispersion relation, derived from TDA equation for separable forces, describing particle-hole collective excitations of the multipolarity λ,

$$\begin{vmatrix} 1-F_\lambda(\pi\pi)S^{(n)}_\pi & -F_\lambda(\pi\nu)S^{(n)}_\nu \\ -F_\lambda(\nu\pi)S^{(n)}_\pi & 1-F_\lambda(\pi\pi)S^{(n)}_\nu\end{vmatrix} = 0, \tag{A8}$$

with the short-hand notation

$$S^{(n)}_\tau = \sum_{j_1j_2}\frac{2q^2_\lambda(\tau j_1j_2)(\epsilon_{\tau j_1}-\epsilon_{\tau j_2})}{(\epsilon_{\tau j_1}-\epsilon_{\tau j_2})^2-\omega^2_\lambda(n)}, \tag{A9}$$

gives the following expression for the proton-neutron interaction:

$$\begin{aligned}F_\lambda(\pi\nu) &= F_\lambda(\nu\pi) \\ &= \sqrt{\frac{[1-F_\lambda(\pi\pi)S^{(n)}_\pi][1-F_\lambda(\nu\nu)S^{(n)}_\nu]}{S^{(n)}_\pi S^{(n)}_\nu}}.\end{aligned} \tag{A10}$$

[1] J. O. Rasmussen, in *Alpha-, Beta- and Gamma-Ray Spectroscopy, Vol. I*, edited by K. Siegbahn (North-Holland, Amsterdam, 1965), p. 701.
[2] I. Tonozuka and A. Arima, Nucl. Phys. A **323**, 45 (1979).
[3] F. A. Janouch and R. J. Liotta, Phys. Rev. C **25**, 2123 (1982).
[4] G. Dodig-Crnkovic, F. A. Janouch, and R. J. Liotta, Phys. Lett. B **139**, 143 (1984).
[5] K. Varga, R. G. Lovas, and R. J. Liotta, Phys. Rev. Lett. **69**, 37 (1992).
[6] D. S. Delion, A. Insolia, and R. J. Liotta, Phys. Rev. C **54**, 292 (1996).
[7] A. Săndulescu, R. Y. Cusson and W. Greiner, Lett. Nuovo Cimento **36**, 321 (1983).
[8] B. Buck, A. C. Merchant, and S. M. Perez, Phys. Rev. Lett. **72**, 1326 (1994).
[9] F. Hoyler, P. Mohr, and G. Staudt, Phys. Rev. C **50**, 2631 (1994).
[10] S. Ohkubo, Phys. Rev. Lett. **74**, 2176 (1995).
[11] B. Buck, A. C. Merchant, and S. M. Perez, Phys. Rev. C **77**, 017301 (2008), and references therein.
[12] E. K. Warburton, Phys. Rev. C **44**, 261 (1991).
[13] A. R. Poletti *et al.*, Nucl. Phys. A **473**, 595 (1987).
[14] A. Astier, P. Petkov, M.-G. Porquet, D. S. Delion, and P. Schuck, Phys. Rev. Lett. **104**, 042701 (2010).
[15] A. Astier, P. Petkov, M.-G. Porquet, D. S. Delion, and P. Schuck, Eur. Phys. J. A **47**, 165 (2010).
[16] Y. Suzuki and S. Ohkubo, Phys. Rev. C **82**, 041303(R) (2010).
[17] P. J. Daly, P. Kleinheinz, R. Broda, S. Lunardi, H. Backe, and J. Blomqvist, Z. Phys. A **298**, 173 (1980).
[18] D. S. Delion and J. Suhonen, Phys. Rev. C **61**, 024304 (2000).
[19] R. J. Liotta and C. Pomar, Nucl. Phys. A **362**, 137 (1981).
[20] V. Gillet, A. M. Green, and E. A. Sanderson, Nucl. Phys. **88**, 321 (1966).
[21] D. S. Delion, *Theory of Particle and Cluster Emission* (Springer-Verlag, Berlin, 2010).
[22] J. Blomqvist and S. Wahlborn, Ark. Fys. **16**, 545 (1960).
[23] P. Ring and P. Schuck, *The Nuclear Many-Body Problem* (Springer-Verlag, Berlin, 1980)
[24] [http://www.nndc.bnl.gov/nudat2/indx_adopted.jsp].
[25] [http://ie.lbl.gov/toi2003/MassSearch.asp].
[26] P. F. Bortignon, R. A. Broglia, D. R. Bes, and R. Liotta, Phys. Rep. C **30**, 305 (1977).
[27] B. Buck, J. C. Johnston, A. C. Merchant, and S. M. Perez, Phys. Rev. C **53**, 2841 (1996).
[28] P. Schuck, Z. Phys. A **279**, 31 (1976).